Geochemical Perspectives Letters

The effect of core segregation on the Cu and Zn isotope composition of the silicate Moon

Y. Xia[1], E.S. Kiseeva[2,3], J. Wade[2*], F. Huang[1*]

Abstract

doi: 10.7185/geochemlet.1928

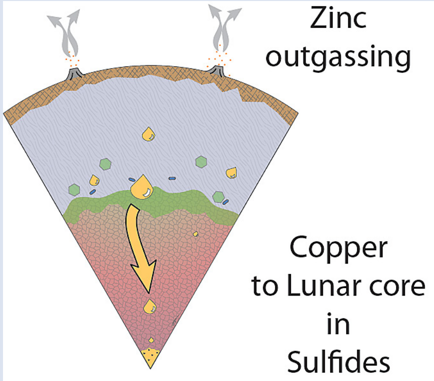

Compared to elements of similar volatility, such as Rb, Ga and K, the bulk silicate Moon (BSM) exhibits significant enrichment in the heavy isotopes of Zn and Cu. However, both elements display a greater affinity for lunar sulfide phases than the other volatiles, suggesting their isotopic abundance in the BSM may also reflect their sequestration to the lunar core. Experimentally determined Cu and Zn isotopic fractionation between liquid metal, sulfide and silicates reveals carbon-bearing iron melts to be isotopically heavier than the silicate melt, and sulfide melts the lightest. During sulfide sequestration from a cooling lunar magma ocean, Cu, unlike Zn, partitions strongly into sulfides ($100 < D_{Cu}^{Sulfide/Melt} < 200$), leaving the BSM both elementally depleted in Cu, and isotopically heavier. Sulfide sequestration therefore explains the larger offsets in the Cu isotope compositions of lunar rocks and the silicate Earth relative to other moderately volatile elements. The lunar Zn isotopic inventory is best explained by volatility driven surface processes. Irrespective of the elemental loss mechanism, the Cu isotopic content of the BSM rules out carbon as a significant light element of the lunar core.

Received 2 July 2019 | Accepted 24 September 2019 | Published 19 November 2019

Introduction

The elemental composition of the bulk silicate Earth and Moon (BSE and BSM respectively) provides insight into the accretion processes and subsequent differentiation of the Earth-Moon system. Lunar rocks and the BSE express many similarities which support a genetic link between the Earth and Moon. These include the proportions of refractory elements and the stable isotope compositions of elements with half-mass condensation temperatures (T_{50}) higher than 1100 K, such as Si (Fitoussi and Bourdon, 2012), Cr (Mougel *et al.*, 2018), and W (Touboul *et al.*, 2007). The Moon does, however, display a notable elemental depletion in the moderately volatile elements, such as Zn, Rb, Ga, K, and Cu, coupled with an enrichment of their heavy isotopes with respect to the BSE (Fig. 1). Although this condensation sequence is for deposition from a reducing nebula gas to solid phases, evaporation from melt at the more oxidising conditions of lunar formation results in Zn and Cu exhibiting similar volatilities (Norris and Wood, 2017). making explanations of their lunar isotopic variability problematic.

These features have been interpreted as resulting from a global scale evaporation event associated with either the giant impact (Wang and Jacobsen, 2016), and/or the differentiation of the Lunar Magma Ocean (LMO) (Day and Moynier, 2014; Kato *et al.*, 2015) and localised degassing of the mare basalt lavas (Sharp *et al.*, 2010). Cu and Zn, however, exhibit larger isotopic variations between mare basalts and the BSE (1.07 ± 0.34 ‰ for Zn, 0.43 ± 0.14 ‰ for Cu) than other volatile isotopes of comparable condensation temperatures (*e.g.*, 0.18 ± 0.2 1 ‰ for Rb, 0.28 ± 0.25 ‰ for Ga, 0.40 ± 0.06 ‰ for K) (Fig. 1). Although element volatility during lunar formation and degassing of the LMO undoubtedly played a role in setting the Moon's elemental and isotopic budget, the disparity between the isotopic and elemental abundances and element condensation temperatures remains enigmatic, suggesting that more than one mechanism may be responsible. We propose that this disparity arises from the segregation of sulfides to the lunar core, exacerbated by the cooling LMO and the consequent decrease in sulfide solubility in silicate melts.

Zinc and copper exhibit both siderophile and chalcophile behaviours, evidenced both by metal-silicate-sulfide partitioning experiments (Siebert *et al.*, 2011; Mahan *et al.*, 2017), and by enrichment in meteorite hosted sulfides (*e.g.*, Williams and Archer, 2011). Geochemical and geophysical studies support the existence of a lunar core exhibiting an extant liquid outer component (Weber *et al.*, 2011), and hence the presence of a significant light element core component.

---

1. CAS Key Laboratory of Crust-Mantle Materials and Environments, School of Earth and Space Sciences, University of Science and Technology of China, Hefei 230026, China
2. Department of Earth Sciences, South Parks Road, Oxford OX1 3AN, UK
3. University College Cork, School of Biological, Earth and Environmental Sciences, Cork, Ireland
* Corresponding authors (email: jon.wade@earth.ox.ac.uk, fhuang@ustc.edu.cn)

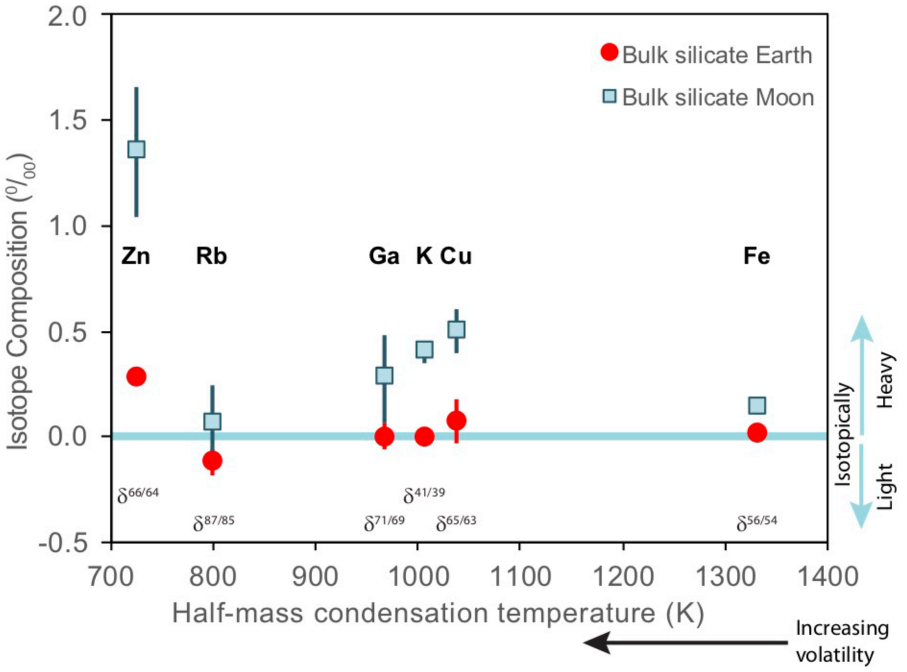

Figure 1 Half-mass condensation temperatures (Lodders, 2003) for a solar system composition gas *versus* isotope composition. Data reference for the isotopic compositions are detailed in the Supplementary Information. It should be noted, however, that the condensation temperatures displayed are for deposition from gas to solid in a nebula gas, not for evaporation from a liquid at the more oxidising conditions pertinent to Moon formation.

Segregation of a metal-rich core from the LMO during lunar core-mantle differentiation, and subsequent mantle cooling and sulfide precipitation (Mavrogenes and O'Neill, 1999), can sequester significant amounts of Cu and, to a lesser extent, Zn, without noticeable influence on lithophile volatiles such as Rb, K, Li, and Ga (Siebert *et al.*, 2011). Given significant Cu isotope fractionation among metallic, silicate, and sulfide melts (Savage *et al.*, 2015), this process will inevitably fractionate lunar Cu isotopes, and, potentially, Zn isotopes. The role of core segregation in shaping the isotope composition of the silicate Moon is, as yet, unclear because equilibrium isotope fractionation factors of Zn and Cu between phases associated with lunar core formation (metal, sulfide, and silicate), remain poorly constrained. Hence, we experimentally explored the equilibrium Zn and Cu isotope fractionation among metallic, sulfide, and silicate melts at conditions relevant to lunar core formation.

Zinc and Copper Isotope Experiments to Simulate LMO Differentiation

We conducted a series of experiments in graphite capsules at 1.5 GPa using piston cylinder apparatus (Tables S-1 to S-4, Fig. S-1 and Methods, see Supplementary Information). The experimental charges contained approximately 50 % silicate of a basaltic composition, equilibrated with ~50 % metal or sulfide with variable Ni content, under fully molten conditions (Tables S-1 to S-5 and Fig. S-1).

For both Cu and Zn isotopes, the iron-rich liquids are slightly enriched in heavier isotopes relative to the silicate melts. In contrast, sulfide melts exhibit demonstrably lighter isotope compositions than the silicate (Fig. 2), with measured Cu isotope fractionation factors consistent with both previous studies of iron meteorites (Williams and Archer, 2011) and experimentally determined Cu isotope fractionation for metal/silicate and sulfide/silicate liquids (Savage *et al.*, 2015) (Table S-6). Zn isotopes display a smaller degree of fractionation than Cu isotopes (Fig. 2). Overall, the isotope fractionation of both elements decreases with increasing temperature. The nickel sulfide content affects the fractionation of both Cu and Zn isotopes (Fig. 2), with high Ni (~25 wt. % Ni in sulfide) experiments exhibiting less fractionation than those with low Ni (0.1 to 1.2 wt. % Ni in sulfide, Table S-1).

Discussion

During lunar core-mantle differentiation, a carbon-bearing, iron-rich core will preferentially sequester isotopically heavy Cu and, potentially Zn, leading to the BSM exhibiting lower (lighter) values in δ^{66}Zn and δ^{65}Cu. This is contrary to observations; the BSM is isotopically heavier than the BSE in both Cu and Zn. Importantly this precludes carbon as a significant light element component of the lunar core. In contrast, sequestration of sulfide to the lunar core would leave the BSM isotopically heavy in both Cu and, potentially Zn, in accordance with the observed offset between silicate Moon and Earth (Fig. 1). It has been proposed that the proto-Moon initially accreted from the outermost volatile-rich disk generated by the giant impact, and is thus less volatile-depleted than the observed lunar rocks from the surface (Canup *et al.*, 2015). Although subsequent degassing of the LMO would result in a significant loss of volatiles from the BSM, its extent would have been mitigated by the presence of an early-formed lunar crust (Elkins-Tanton and Grove, 2011). The lunar interior may therefore have retained abundant volatiles, including sulfur, through inefficient degassing, as evidenced by the comparable sulfur content of lunar magmas and terrestrial mid-ocean ridge basalts (Hauri *et al.*, 2017). In comparison to analogous terrestrial basalts, the solubility of sulfide in the melt decreases as the BSM undergoes secular cooling, exacerbated by the lunar mantle's lower oxygen fugacity (O'Neill and Mavrogenes, 2002), promoting the formation of an immiscible sulfide liquid.

To explore this mechanism and its effect on Zn and Cu isotopic signatures, we calculated the $\delta^{66/64}$Zn and $\delta^{65/63}$Cu content of the BSM by considering the scenario of sulfide

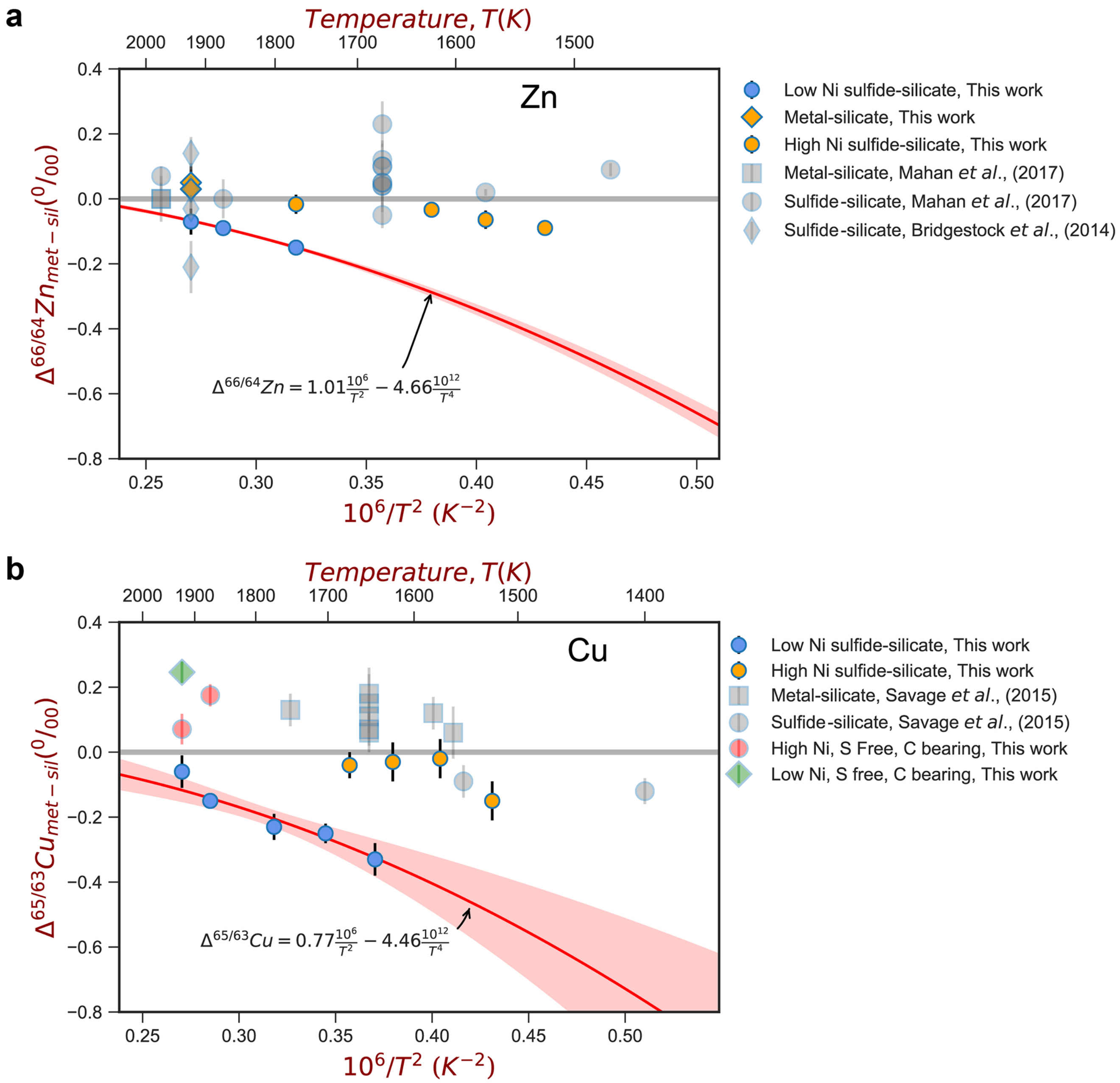

Figure 2 **(a,b)** Zn and Cu isotope fractionation factors between liquid metal-silicate and sulfide-silicate as a function of temperature. Both increasing temperature and Ni content of sulfide decrease the Zn and Cu isotope fractionation, with the result that low Ni sulfides all exhibit a temperature dependent excess of isotopically light Cu and Zn. The pale-red band is the 95 % confidence interval for the regression shown.

segregation from an ambient basaltic magma ocean and assuming the bulk Moon is predominantly comprised of material derived from the Earth's mantle (Canup, 2012; Wade and Wood, 2016).

Under the conditions of lunar sulfide sequestration, Cu, unlike Zn, exhibits a strong preference for the sulfide phase; the lunar Cu sulfide/silicate partition coefficient, $D_{Cu\text{-}Moon}^{Sulfide/Silicate}$, ranges from 100 to 200, in contrast to Zn, which is ~1 (Kiseeva and Wood, 2015). This results in a sulfide liquid, initially in equilibrium with the silicate LMO prior to its sequestration to the lunar core, enriched in isotopically light Cu. This leads to a BSM exhibiting a significant depletion in Cu and becoming isotopically heavy in Cu. The result is a divergence of Cu isotopes between the BSE and BSM, with a negligible effect on isotopes of lithophile elements (*e.g.*, Rb, Ga, and K). Zn, however, exhibits negligible elemental and isotopic fractionation upon lunar sulfide extraction; a consequence of both its lower isotopic fractionation and chalcophile behaviour. The limited Zn isotope fractionation that occurs during the evolution of mafic magma (Chen *et al.*, 2013), coupled with the uniform $\delta^{66/64}$Zn in high Ti (1.50 ± 0.54 ‰, n = 17) and low Ti lunar basalts (1.35 ± 0.43 ‰, n = 17), suggest their Zn isotope compositions reflect that of the primitive lunar magmas (Kato *et al.*, 2015). During terrestrial mantle melting, high degrees of melt extraction (>30 %) may fractionate Zn isotopes up to 0.16 ‰ (Doucet *et al.*, 2016). The significantly lower melt extraction (~5-11 %) expressed by the mare basalts (Day and Walker, 2015) will consequently yield only subtle isotopic variations in Zn, negligible relative to the large offset between the BSE and lunar rocks.

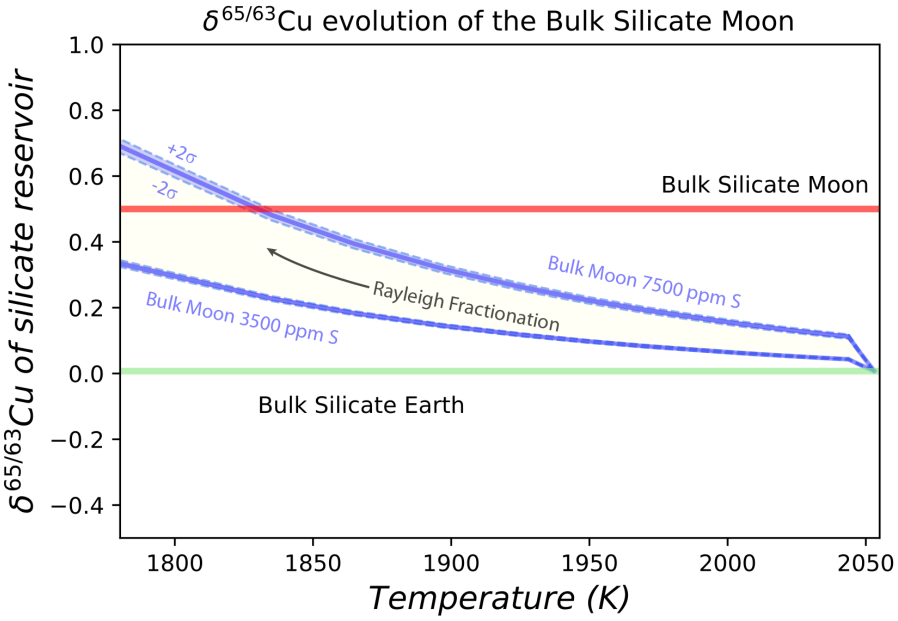

Figure 3 The Cu isotope evolution of the silicate Moon during lunar sulfide segregation. Assuming the Moon is derived from the precursor BSE, and the Moon's core is predominantly FeS (equating to a bulk Moon of ~7500 ppm S), or just the outer core (3500 ppm S) and sulfide sequestration occurs by Rayleigh fractionation, the silicate Moon becomes progressively lighter in Cu. Horizontal lines represent values of the BSM estimated by lunar basalts (red) and the BSE (green) (Herzog *et al.*, 2009). The pale blue band represents 2 standard deviations of the error on the mean of the fractionation regression.

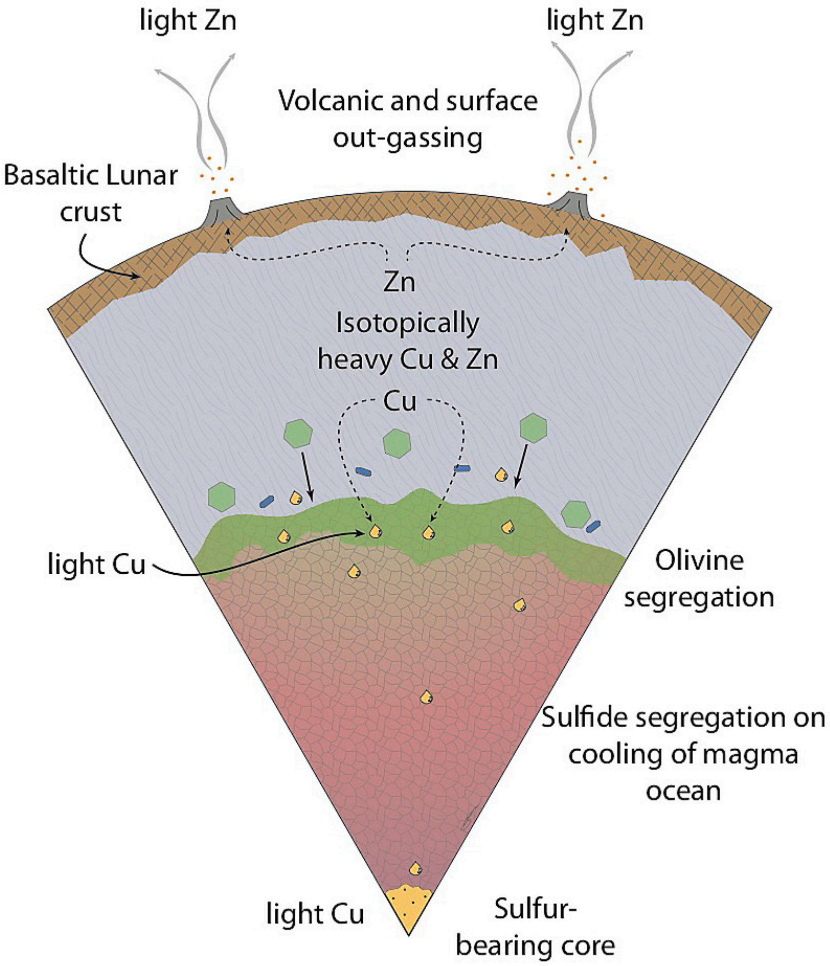

Figure 4 Cu is hosted in lunar sulfides as a consequence of its significantly higher preference for the sulfide phase over silicate during LMO cooling and the consequent decreasing solubility of sulfide in the melt. Zn, however, is little affected implying the BSM Zn isotopic content is set by element volatility during Moon formation and LMO degassing. The BSM's Cu isotopic composition reflects sulfide loss to the lunar core.

Modelling sulfide segregation by Rayleigh fractionation reveals that sulfur-rich lunar core formation cannot be responsible for the isotopically heavy $\delta^{66/64}$Zn BSM, nor for its elemental depletion. Given the limited mineralogical host phases for Zn, the most likely mechanism of lunar Zn depletion is that of volatility during lunar formation (Paniello *et al.*, 2012) or magma ocean degassing (Kato *et al.*, 2015). In contrast, the silicate Moon's high $\delta^{65/63}$Cu can be explained as a direct consequence of sulfide sequestration to the core (Fig. 3), a result of the initially molten Moon saturated in FeS and exacerbated by the subsequent drop in the sulfide content of lunar magmas on cooling (Mavrogenes and O'Neill, 1999). In addition, sulfide sequestration depletes the silicate Moon in the chalcophile elements Cu and Ni (Walter *et al.*, 2000), without significantly disturbing the W isotopic age of the Moon (Wade and Wood, 2016), an element that displays little affinity for the sulfide phase.

Sulfide retained in the deep Moon may therefore be an important reservoir for isotopically light Cu, but not Zn, which is best explained by its volatility during the Moon forming impact and subsequent degassing from the Lunar crust (Fig. 4.). The silicate Earth and Moon share almost identical Cr isotope compositions (Mougel *et al.*, 2018), an element marginally more volatile than Fe (1296 K and 1334 K half-mass condensation temperatures respectively (Lodders, 2003)), but which exhibits a similar sulfide/melt partitioning behaviour to Zn (Kiseeva and Wood, 2015). Therefore, the segregation of sulfide (Brenan and Mungall, 2017) can drive the silicate Moon to Cu isotopic compositions, but this process has little effect on elements which display a lower preference for lunar sulfides, such as Zn and Cr. Compared to the BSE, the silicate Moon exhibits around a threefold depletion in Ni (Walter *et al.*, 2000), an observation consistent with its extraction during lunar core formation *via* sulfide segregation (Wade and Wood, 2016). Assuming the Moon's Ni content is inherited primarily from the silicate Earth, this suggests the Moon's core contains around 7.5 wt. % Ni. Increasing metallic Ni contents implies higher core sulfur contents for a given Cu isotope content exhibited by the silicate Moon.

Sulfide saturation may arise from the secular cooling of a LMO containing excess sulfide derived from the Moon forming impactor, and/or the late addition of S to the lunar mantle. Because of the higher density of sulfide relative to the ambient magma, and the initially completely molten lunar mantle, excess or precipitating sulfide will sink into the lunar interior. The near-chondritic ^{187}Os/^{188}Os and chondrite-relative HSE abundance in high MgO mare basalts (Day and Walker, 2015) implies that this sulfide component is efficiently extracted from the silicate Moon to the Lunar core, with little stranded in the source region of the Mare basalts (Brenan and Mungall, 2017). This addition of sulfide liquid to lunar core is in line with the studies that propose sulfur as a dominant light element in the lunar core (Rai and van Westrenen, 2014).

Acknowledgements

This work is supported by the Strategic Priority Research Program (B) of Chinese Academy of Sciences (Grant No. XDB18000000), the National Science Foundation of China (41325011, 41630206). ESK was supported by NERC grant NE/L010828/1. JW acknowledges receipt of a NERC Independent Research Fellowship NE/K009540/1. We thank Huimin Yu and Xingchao Zhang for the help of Zn and Cu isotope analyses.

Editor: Helen Williams

Author Contributions

FH and ESK conceived the experimental study. ESK performed the high pressure experiments. ESK and YX conducted the electron probe measurement. YX and FH processed the samples and performed the SEM, LA-ICP-MS, and MC-ICP-MS analyses. JW performed EPMA/SEM analysis on the C-bearing samples, conceived the application, performed the data modelling and presentation. All authors contributed to interpretation of the data and writing the paper.

Additional Information

Supplementary Information accompanies this letter at http://www.geochemicalperspectivesletters.org/article1928.

Cite this letter as: Xia, Y., Kiseeva, E.S., Wade, J., Huang, F. (2019) The effect of core segregation on the Cu and Zn isotope composition of the silicate Moon. *Geochem. Persp. Let.* 12, 12–17.

References

Bridgestock, L.J., Williams, H., Rehkämper, M., Larner, F., Giscard, M.D., Hammond, S., Coles, B., Andreasen, R., Wood, B.J., Theis, K.J., Smith, C.L., Benedix, G.K., Schönbächler, M. (2014) Unlocking the zinc isotope systematics of iron meteorites. *Earth and Planetary Science Letters* 400, 153-164.

Brenan, J.M., Mungall, J.E. (2017) A sulfide-saturated lunar mantle? *2017 EGU General Assembly, Geophysical Research Abstracts* 19, EGU2017-6838.

Canup, R.M. (2012) Forming a Moon with an Earth-like Composition via a Giant Impact. *Science* 338, 1052-1055.

Canup, R.M., Visscher, C., Salmon, J., Fegley Jr, B. (2015) Lunar volatile depletion due to incomplete accretion within an impact-generated disk. *Nature Geoscience* 8, 918-921.

Chen, H., Savage, P.S., Teng, F.-Z., Helz, R.T., Moynier, F. (2013) Zinc isotope fractionation during magmatic differentiation and the isotopic composition of the bulk Earth. *Earth and Planetary Science Letters* 369, 34-42.

Day, J.M., Moynier, F. (2014) Evaporative fractionation of volatile stable isotopes and their bearing on the origin of the Moon. *Philosophical Transactions of the Royal Society A* 372, 20130259.

Day, J.M., Walker, R.J. (2015) Highly siderophile element depletion in the Moon. *Earth and Planetary Science Letters* 423, 114-124.

Doucet, L.S., Mattielli, N., Ionov, D.A., Debouge, W., Golovin, A.V. (2016) Zn isotopic heterogeneity in the mantle: A melting control? *Earth and Planetary Science Letters* 451, 232-240.

Elkins-Tanton, L., Grove, T. (2011) Water (hydrogen) in the lunar mantle: Results from petrology and magma ocean modeling. *Earth and Planetary Science Letters* 307, 173-179.

Fitoussi, C., Bourdon, B. (2012) Silicon isotope evidence against an enstatite chondrite Earth. *Science* 335, 1477-1480.

Hauri, E.H., Saal, A.E., Nakajima, M., Anand, M., Rutherford, M.J., Orman, J.A.V., Voyer, M.L. (2017) Origin and Evolution of Water in the Moon's Interior. *Annual Review of Earth and Planetary Sciences* 45, 89-111.

Herzog, G., Moynier, F., Albarède, F., Berezhnoy, A. (2009) Isotopic and elemental abundances of copper and zinc in lunar samples, Zagami, Pele's hairs, and a terrestrial basalt. *Geochimica et Cosmochimica Acta* 73, 5884-5904.

Kato, C., Moynier, F., Valdes, M.C., Dhaliwal, J.K., Day, J.M.D. (2015) Extensive volatile loss during formation and differentiation of the Moon. *Nature Communications* 6, 7617.

Kiseeva, E.S., Wood, B.J. (2015) The effects of composition and temperature on chalcophile and lithophile element partitioning into magmatic sulphides. *Earth and Planetary Science Letters* 424, 280-294.

Lodders, K. (2003) Solar System Abundances and Condensation Temperatures of The Elements. *Astrophysical Journal* 591, 1220-1247.

Mahan, B., Siebert, J., Pringle, E.A., Moynier, F. (2017) Elemental partitioning and isotopic fractionation of Zn between metal and silicate and geochemical estimation of the S content of the Earth's core. *Geochimica et Cosmochimica Acta* 196, 252-270.

Mavrogenes, J.A., O'Neill, H.S.C. (1999) The relative effects of pressure, temperature and oxygen fugacity on the solubility of sulfide in mafic magmas. *Geochimica et Cosmochimica Acta* 63, 1173-1180.

Mougel, B., Moynier, F., Göpel, C. (2018) Chromium isotopic homogeneity between the Moon, the Earth, and enstatite chondrites. *Earth and Planetary Science Letters* 481, 1-8.

Norris, C.A., Wood, B.J. (2017) Earth's volatile contents established by melting and vaporization. *Nature* 549, 507.

O'Neill, H.S.C., Mavrogenes, J.A. (2002) The sulfide capacity and the sulfur content at sulfide saturation of silicate melts at 1400 C and 1 bar. *Journal of Petrology* 43, 1049-1087.

Paniello, R.C., Day, J.M., Moynier, F. (2012) Zinc isotopic evidence for the origin of the Moon. *Nature* 490, 376-379.

Rai, N., van Westrenen, W. (2014) Lunar core formation: New constraints from metal–silicate partitioning of siderophile elements. *Earth and Planetary Science Letters* 388, 343-352.

Savage, P.S., Moynier, F., Chen, H., Shofner, G., Siebert, J., Badro, J., Puchtel, I. (2015) Copper isotope evidence for large-scale sulphide fractionation during Earth's differentiation. *Geochemical Perspectives Letters* 1, 53-64

Sharp, Z., Shearer, C., Barnes, J. (2010) The chlorine isotope composition of the Moon. *41st Lunar and Planetary Science Conference*, Abstract 2424.

Siebert, J., Corgne, A., Ryerson, F.J. (2011) Systematics of metal–silicate partitioning for many siderophile elements applied to Earth's core formation. *Geochimica et Cosmochimica Acta* 75, 1451-1489.

Touboul, M., Kleine, T., Bourdon, B., Palme, H., Wieler, R. (2007) Late formation and prolonged differentiation of the Moon inferred from W isotopes in lunar metals. *Nature* 450, 1206-1209.

Wade, J., Wood, B.J. (2016) The oxidation state and mass of the Moon-forming impactor. *Earth and Planetary Science Letters* 442, 186-193.

Walter, M.J., Newsom, H.E., Ertel, W., Holzeid, A. (2000) Siderophile elements in the Earth and Moon: metal/silicate partitioning and implications for core formation. In: Canup, R.M., Righter, K. (Eds.) *Origin of the Earth and Moon*. University of Arizona Press, Tucson, 265-289.

Wang, K., Jacobsen, S.B. (2016) Potassium isotopic evidence for a high-energy giant impact origin of the Moon. *Nature* 538, 487-490.

Weber, R.C., Lin, P.Y., Garnero, E.J., Williams, Q., Lognonne, P. (2011) Seismic detection of the lunar core. *Science* 331, 309-312.

Williams, H.M., Archer, C. (2011) Copper stable isotopes as tracers of metal–sulphide segregation and fractional crystallisation processes on iron meteorite parent bodies. *Geochimica et Cosmochimica Acta* 75, 3166-3178.

Geochemical Perspectives Letters

Published by the European Association of Geochemistry

The effect of core segregation on the Cu and Zn isotope composition of the silicate Moon

Y. Xia, E.S. Kiseeva, J. Wade, F. Huang

Supplementary Information

The Supplementary Information includes:

- Petrological Experiments
- Electron Microprobe analysis
- Laser Ablation ICPS analysis
- Isotopic Analysis
- Modelling the Effect of Sulfide Sequestration on the Isotopic Content of the Silicate Moon
- Additional Information in Support of Figure 1
- Figures S-1 to S-4
- Tables S-1 to S-6
- Supplementary Information References

Petrological Experiments

All experiments were performed at 1.5 GPa under fully molten conditions (Table S-1) using a Boyd-England type end-loaded piston-cylinder apparatus at the Department of Earth Sciences, University of Oxford. For all experiments either a ½-inch CaF_2 pressure media (for temperatures below 1450 ˚C) or a ½-inch $BaCO_3$–SiO_2 glass (for temperatures 1450 ˚C and above) assembly with a graphite heater was used (*e.g.*, McDade *et al*., 2002). The internal spacers consisted of crushable, MgO, fired at 1000 °C to ensure dryness, and the capsule consisted of high density, spectroscopically pure graphite, 6 mm in outer diameter and 3x3 mm inner dimensions. Experimental temperatures were controlled using $W_{95}Re_5$–$W_{74}Re_{26}$ thermocouples separated from the capsule by a 0.5 mm alumina disc. Temperature ranges from 1250 to 1650 °C for sulfide-silicate experiments and 1500 to 1650 °C for metal-silicate experiments (Table S-1). Duration ranged from 30 to 180 min (Table S-1), shown to be adequate for attaining isotope exchange equilibrium at similar P-T conditions (Bridgestock *et al*., 2014; Mahan *et al*., 2017). Run durations are varied roughly as a function of temperature, with generally shortened duration at elevated temperature. Experimental products were quenched by cutting power to the resistive furnace whilst run pressure was maintained. During quenching, the experiment cools to beneath the silicate solidus in 2-3 s.

Starting materials were synthetic basalt rock powder, doped with Cu and Zn (Zn as ZnO, Cu as either Cu_2O or Cu_2S), equilibrated with metal or sulfide with variable Ni content (Tables S-2 to S-4), in approximately co-equal mixtures by weight of synthetic sulfide/silicate or metal/silicate. The starting materials were loaded into the graphite capsules; these were found to minimise the potential for Zn loss during the experiment and also aid in the extraction of the run products. Run products were extracted by cutting open the capsule using a diamond wire saw, before setting a small part into epoxy resin prior to polishing for texture and elemental composition analyses, with the majority used for isotope analysis.

Electron Microprobe Analysis

All experimental products were analysed using a Jeol JXA-8100 electron microprobe using wavelength dispersive spectroscopy (WDS) at the Key Laboratory of Submarine Geosciences, State Oceanic Administration. Analytical conditions were set at 15 kV/20 nA, with a 1 μm spot used for silicate analysis, and 20 kV/20 nA, 10 μm defocused spot utilised for metal and sulfide measurement to better sample areas with heterogeneities. Spectrometers were calibrated for peak position and intensity on a range of natural mineral standards. Peak and background counting time were 10 s for major elements each element. Na, Si, Al, and Mg were run on TAP, K and Ca were run for PETH, Fe, Cr, Mn, Ti, and Ni were analysed on the LIF crystal. Minerals, oxides, pure metals, and pure sulfide were used as standards for all elements. Some samples were repeatedly analysed using a JEOL JXA8600 electron microprobe at the Department of Archaeology at the University of Oxford. WDS analyses were performed using a 15 kV accelerating voltage (15 kV_{acc}) and 20 to 40 nA beam current with a defocused 10-micron beam size. A detailed description can be found in Kiseeva and Wood (2013). Data obtained from the two labs are consistent within error, therefore only the WDS measurements analysed in the Laboratory of Submarine Geosciences are reported. High standard deviations of sulfide phases are due to the heterogeneous quenching of Ni- and Cu- bearing sulfides (Table S-2). The iron bearing experiments (IS7-1, -2, and IS5-2, Fig. S-1) resulted in the metallic component being saturated in carbon. The carbon contents of these experiments were calculated from the Fe-C phases diagram, summarised by Wood, 1993, using the online calculator hosted at http://norris.org.au/expet/metalact/. Major and minor element analysis was performed at Oxford using a Cameca SX5FEG microprobe, 20 kV_{acc} and 20 nA beam, with standards again a range of oxides and metals.

Laser Ablation ICPMS (LA-ICPMS) analysis

Minor and trace element compositions of the quenched silicate melt were determined using an Agilent 7700e ICPMS coupled with a GeolasPro ArF (193 nm) excimer laser sampling system at the Chinese Academy of Sciences Key Laboratory of crust-mantle Materials and Environments, University of Science and Technology of China (USTC), Hefei, China. A calibration strategy of total metal-oxide normalisation (Liu *et al*., 2008) was adopted. Beam diameters of 44 μm were used. More detail about analytical procedures and parameters can be found in He *et al*. (2016). USGS reference glasses possessing comparable compositions with our basaltic silicate glasses including BCR-2, BHVO-1, and BIR-1, were used for external calibration. Analyses of the reference glasses generally agree with the recommended values (https://crustal.usgs.gov/geochemical_reference_standards/microanalytical_RM.html) within 10 % (relative standard deviation, RSD) for minor and trace elements. Compositions for the quenched silicate melt analysed using LA-ICPMS (Table S-4) agree within analytical error those measured by EMPA (Table S-3).

Isotopic Analyses

In previous comparable experiments, no isotopic fractionation of zinc was observed (Bridgestock *et al*., 2014; Mahan *et al*., 2017), mainly due to the relatively large analytical uncertainties caused by error propagation when using the traditional sample-standard bracketing approach (Fig. 2a). To reduce the uncertainty on Zn isotope fractionation, we bracketed the coexisting experimental phases when calculating the isotope fractionation between the two associated silicate and metal/sulfide phases (see Methods). The improved precision (Table S-5) achieved using this method allows clear resolution of the zinc isotope differences between the co-existing phases (Fig. 2a), however, both methods result in fractionation factors that are identical within error (Figs. S-3). For ease of comparison with previously published data we have therefore chosen to use the Cu data derived from the sample-standard bracketing approach.

Chemical purification

The remaining part of each run product was lightly crushed in agate mortar and pestle. Metal, sulfide, and silicate phases were manually separated using optical microscopy and magnets. Cu is both chalcophile and siderophile and Zn is chalcophile and slightly siderophile, such that any contamination from sulfide and metal may alter both the concentration and isotopic signature of the silicate. The silicate fractions were therefore checked for purity with caution by repeating the separation process for several times, and those with magnetic or microscopically visible metal or sulfide were dismissed to minimise cross-contamination for isotope analyses.

The separated phases (silicate, metal, and sulfide fractions) were cleaned prior to digestion to remove any possible surface contamination, by treating with ethanol (3 times, each 15 min), followed by 18.2 MΩ cm Milli-Q H_2O (3 times, each 15 min) in an ultrasonic bath. Dissolution of silicate phase involved three steps using double-distilled, concentrated acids: a 3:1 mixture of HF-

HNO_3; a mixture of HCl-HNO_3; and 1 ml HCl. Metal and sulfide phases were dissolved following the latter two processes. Dissolutions were conducted in closed Savillex beakers on a hot plate at 100 ℃ and were then dried down before the addition of new acids. After full digestion, the samples were dissolved in 6M HCl for major and trace element measurement and column chemistry.

Both purifications of Zn and Cu were achieved by chromatography using anion exchange resin (AG MP−1M, 100–200 mesh), which has high partition coefficients for them at low PH in chloride form. Chemical purification for Zn followed procedures from Chen *et al.* (2016). Samples were dissolved in 1 mL 6M HCl and loaded on to the columns filled with 2 ml resin. Zn was absorbed to the resin as chlorine complex while most other cationic species are eluted with 0.5 HCl. Zn is subsequently eluted using 0.5 N HNO_3. A second separation step with 0.5 ml resin was performed for further purification. Column chemistry of Cu utilised the procedures established by Huang *et al*. (2017). After sample loading onto the column in 1 ml of 6M HCl + 0.001 % H_2O_2, matrix elements were then eluted by 5 ml of 6M HCl + 0.001 % H_2O_2. The Cu was eluted in a further 26 ml of Ml + 0.001 % H_2O_2. The whole procedure was repeated for further purification. Both Cu and Zn yields were checked using ICPMS and proved to be >99.5 %.

Multicollector-ICPMS (MC-ICPMS)

Both Cu and Zn isotopic analyses were performed on a Thermo Scientific Neptune Plus MC–ICPMS in low-resolution mode at USTC. The final sample was dissolved in 2 % HNO_3 and introduced into the instrument using an ESI PFA microflow nebulizer with an uptake rate of (50 µL min^{-1} flow rate). Zinc isotopes were analysed using the techniques described in Chen *et al*. (2016). The yields exceeded 99 %. Isotope ratios are expressed in δ–notation, relative to the NIST SRM 683 standard:

$$\delta^{j/64}Zn_{SRM683} = [(^{j}Zn/^{64}Zn)_{sample} / (^{j}Zn/^{64}Zn)_{SRM683} - 1] \times 1000\ (‰),$$

where j refers to mass 66 or 68. Total procedural Zn and Cu blanks were ca. 5 and <10 ng, respectively, insignificant relative to the amounts of Cu (1-10 µg) and Zn (1-4 µg) onto columns. USGS standards (see Table S-5) were treated along with the samples to test method accuracy. For inter-lab comparison, Zn isotope compositions of USGS standards were calculated as a deviation from JMC–Lyon ($\delta^{j}Zn_{JMC\text{-}Lyon}$) by adding the offset between SRM683 and JMC–Lyon, +0.125 ‰ for $\delta^{66/64}Zn$ and 0.258 ‰ for $\delta^{68}Zn$, based on long-term measurement. Total procedural Zn blank was <10 ng, insignificant relative to the amounts of Zn (1-4 ug) onto columns. Our data for USGS standards (Table S-6) are in excellent agreement with previously published data within error (Moynier *et al*., 2017 and references therein). To assess method reproducibility, several sample aliquots were separated into two parts; each part was separately processed through column chemistry and analyses. These repeats have identical values within error. A number of samples are repeated by dissolving a new quality of powder; again, these re-dissolutions have the sample isotope compositions (Table S-6).

For Cu isotope analyses, ^{63}Cu and ^{65}Cu isotope beams were collected in C and L2 faraday cups, respectively. Matrix elements were monitored using ^{62}Ni and ^{64}Zn beams in L3 and L1 in the same cup setup. Under typical running conditions, a 250 ppb Cu solution generated ca. 5V total signal. To correct for instrumental mass bias, isotope measurements were calculated using the sample standard bracketing protocol relative to the NIST SRM 976 standard, whereby variation in isotopic composition is defined using $\delta^{65/63}Cu$ as follows:

$$\delta^{65/63}Cu = [(^{65}Cu/^{63}Cu)_{sample} / (^{65}Cu/^{63}Cu)_{SRM\ 976} - 1] \times 1000\ (‰)$$

Each sample $\delta^{65/63}Cu$ is the average of 3 analyses. Instrumental drift was monitored using two mono-elemental reference materials ERM-AE-647 and AAS, $\delta^{65/63}Cu$ of which are 0.19±0.05 ‰ (2 SD, n= 347) and 0.30± 0.05 ‰ (2SD, n= 51) respectively. Analyses of them yielded a long-term external precision of $\delta^{65/63}Cu$ better than 0.05 ‰ (2 SD, 95 % confidence interval). Total procedural Cu was <5 ng, insignificant relative to the amounts of Cu (1-10 µg) onto columns. Data for USGS standards treated along with the samples agree with previously published data (Moynier *et al*., 2017 and references therein) within error. Both sample aliquots and sample powder splits exhibit consistent value (Table S-6).

The offset of isotope compositions of the coexisting phases was treated as isotope fractionation factor for Zn and Cu, the uncertainty of which was obtained by error propagation. Specifically, the Zn (or Cu) purified from the coexisting phases were bracketing mutually, acting as standard and sample in the standard bracketing techniques, respectively. The advantage of this technique is that it provides high precision under routine instrument running conditions. Therefore, it provides the possibility to discriminate tiny fractionation approximate analytical error of the traditional method. A similar method was adopted by Pringle and Moynier (2017) to discriminate the slight difference in Rb isotope compositions between the lunar samples and terrestrial rocks by using the terrestrial basalt, BCR-2, as the bracketing standard. The isotope fractionation factor acquired from both methods are identical within error (Tables S-5 and S-6), demonstrating the reliability of our data. The fractionation factor was obtained by linear regression (Figs. 2a & b), of the form $a/T^2+b/T^4$ (T is temperature in kelvin), with model selection made by using that with the lowest BIC (Bayesian information criteria) score.

Modelling the Effect of Sulfide Sequestration on the Isotopic Content of the Silicate Moon

Elemental and isotopic partitioning between silicate and metallic phases is a function of a range of physico-chemical parameters, including temperature, pressure and compositional factors. Lunar formation resulting from a giant impact implies that the pressures of lunar core-mantle differentiation may occur over pressures ranging up to that of the present lunar core mantle boundary (~4.9 GPa) (Righter and Drake, 1996). On the other hand, experimentally derived core-mantle partition coefficients for Cu and Zn are relatively insensitive across the putative pressure range of lunar core formation (*e.g.* Kiseeva and Wood, 2015). For simplicity, the following calculations therefore use a mean core-mantle equilibration pressure of 1.5 GPa, with the advantage that experimentally derived fractionation factors are not affected by the assumed pressures of lunar core formation. Sulfide composition plays a dominant role in setting the elemental partition coefficient, $D^{i}_{sul/sil}$, and temperature determines the isotopic fractionation factor; $\Delta^{i}_{sul/sil}$. $D^{i}_{sul/sil}$ is calculated according to the parameterisation of Kiseeva and Wood (2015), with the BSM FeO content of 9-13 wt. % taken from Wade and Wood (2016) and a normalised terrestrial pyrolite composition taken as the major element composition of the BSM (McDonough and Sun, 1995). We adopt the temperatures of the lunar core formation between 1400 and 1850 ℃, within previously estimated range of 1400 to 1900 ℃ (Righter and Drake, 1996); the silicate melt was fractionally crystallised using Petrolog (Danyushevsky and Plechov, 2011) and the sulfide content of the silicate melt at sulfide saturation calculated using Smythe *et al.* (2017). The temperature dependence of Cu and Zn isotope fractionation factors were calculated (Fig. 2), based on the data derived from the low-Ni experiments, and used to extrapolate the fractionation factor over the full range of temperatures. The size fraction of the lunar core is taken as ~1.6 wt. % by mass (F_{core}) (Weber *et al*., 2011).

Because extrapolation of the models to temperatures significantly above the experimental range are potentially prone to artefacts (in particular, elevated carbon contents of the metallic phases and ingress of the run products into the capsule), the lunar model presented here is founded on the experimental pressures and temperatures. The models developed here therefore represent minimum lunar core S contents and reinforce the general conclusions of a sulfur rich, carbon deplete lunar core.

Additional Information in Support of Figure 1

The isotopic data shown in Figure 1 was taken from the following sources: Zn (Paniello *et al*., 2012; Kato *et al*., 2015), Rb (Pringle and Moynier, 2017), Ga (Kato and Moynier, 2017), K (Wang and Jacobsen, 2016), Cu (Herzog *et al*., 2009; Savage *et al*., 2015) and Fe (Craddock *et al*., 2013; Elardo and Shahar, 2017)

Supplementary Tables

Table S-1 Experimental conditions.

Run #	Starting composition	Doped with elements	Temperature (°C)	Duration (min)
IS5-2	50 % KK3 basalt + 50 % Fe + traces	Cu_2O, ZnO	1650	30
IS7-1	50 % KK3 basalt + 40 % Fe + 10 % Ni + traces	Cu_2O, ZnO	1600	30
IS7-2	50 % KK3 basalt + 40 % Fe + 10 % Ni + traces	Cu_2O, ZnO	1650	30
Cu 2-2	50 % KK3 basalt + 50 % FeS + traces	Cu_2O, NiO	1370	60
Cu 2-3	50 % KK3 basalt + 50 % FeS + traces	Cu_2O, NiO	1430	30
IS3-1	50 % KK3 basalt + 50 % FeS + traces	Ni_3S_2, Cu_2S, ZnO	1500	60
IS3-2	50 % KK3 basalt + 50 % FeS + traces	Ni_3S_2, Cu_2S, ZnO	1600	30
IS4-1	45 % KK3 basalt + 30 % FeS + 20 % Ni_3S_2 + 5 % orthoclase + traces	Cu_2S, ZnO	1400	180
IS4-2	45 % KK3 basalt + 30 % FeS + 20 % Ni_3S_2 + 5 % orthoclase + traces	Cu_2S, ZnO	1350	180
IS4-3	45 % KK3 basalt + 30 % FeS + 20 % Ni_3S_2 + 5 % orthoclase + traces	Cu_2S, ZnO	1300	150
IS4-4	45 % KK3 basalt + 30 % FeS + 20 % Ni_3S_2 + 5 % orthoclase + traces	Cu_2S, ZnO	1250	180
IS4-6	45 % KK3 basalt + 30 % FeS + 20 % Ni_3S_2 + 5 % orthoclase + traces	Cu_2S, ZnO	1500	60
KK54	50 % KK3 basalt + 50 % FeS + traces	Cu_2S, ZnO	1650	30

All runs were conducted at 1.5 GPa.
Graphite capsules were used for all experiments.
KK3 basalt is a synthetic MORB.

Table S-2 Major element compositions (in wt. %) of the metal and sulfide phases measured by EPMA.

Run #	n	Fe	σ	S	σ	Cu	σ	Ni	σ	Zn	σ	Si	σ	total	XC*
IS5-2	46	91.80	0.50	0.04	0.01	2.45	0.23	b.d.l.	-	0.50	0.06	-	-	94.80	0.21
IS7-1	55	77.71	1.55	0.04	0.02	1.37	0.22	15.68	1.28	0.52	0.11	-	-	95.32	0.185
IS7-2	45	75.66	2.07	0.05	0.02	1.27	0.21	17.08	1.56	0.57	0.11	-	-	94.63	0.188
Cu2-2	3	58.31	2.84	32.92	1.48	5.58	2.56	1.10	0.16	-	-	b.d.l.	-	97.91	-
Cu2-3	5	59.65	0.86	33.79	1.01	3.39	1.04	1.24	0.06	-	-	b.d.l.	-	98.07	-
IS3-1	7	62.53	0.37	36.25	0.16	0.41	0.01	0.07	0.02	0.04	0.02	0.03	0.01	99.33	-
IS3-2	9	62.41	0.29	36.19	0.38	0.35	0.03	0.06	0.02	0.05	0.02	0.10	0.06	99.16	-
IS4-1	4	42.48	7.24	32.59	1.31	0.75	0.22	21.41	8.24	-	-	b.d.l.	-	97.25	-
IS4-2	10	35.32	6.15	34.41	3.37	1.94	1.22	26.21	6.30	-	-	b.d.l.	-	98.05	-
IS4-3	8	36.31	3.5	32.45	1.11	1.22	0.46	28.7	4.51	0.13	0.16	0.04	0.01	98.82	-
IS4-4	7	36.85	1.68	32.94	0.89	1.32	0.73	27.94	1.78	0.11	0.19	0.04	0.03	99.21	-
IS4-6	10	35.99	2.88	32.16	1.39	0.98	0.58	29.01	2.93	-	-	0.08	0.05	98.22	-
KK54	11	60.27	1.05	36.73	1.17	0.97	0.14	0.1	0.04	0.15	0.05	0.12	0.04	98.34	-

b.d.l. – below detection limit.

*Mole fraction of carbon in the metallic phase calculated, where present, from the Fe-C phase diagram, summarised by Wood (1993).

For further details, see the online calculator made available at http://norris.org.au/expet/metalact/

Table S-3 Major element compositions (in wt. %) of quenched silicate melt measured by EPMA.

Run #	n	Na_2O	σ	K_2O	σ	SiO_2	σ	Al_2O_3	σ	MgO	σ	CaO	σ	Cr_2O_3	σ	FeO	σ	TiO_2	σ	P_2O_5	σ	ZnO	σ	SO_3	σ	Total	Trace elements*
IS5-2	17	1.78	0.09	0.14	0.01	47.1	0.5	14.74	0.18	10.07	0.16	11.19	0.2	0.01	0.01	10.85	0.38	0.7	0.1	b.d.l.	-	2.55	0.16	0.02	0.01	99.38	0.22
IS7-1	55	2.08	0.09	0.15	0.01	47.16	0.38	15.09	0.09	10.07	0.12	12.01	0.09	-	-	10.28	0.07	0.79	0.02	-	-	2.07	0.03	0.04	0.03	99.95	-
IS7-2	45	2.09	0.09	0.16	0.01	47.88	0.22	15.07	0.09	10.15	0.06	12.05	0.06	-	-	10.13	0.07	0.79	0.02	-	-	2.09	0.03	0.04	0.02	100.65	-
Cu2-2	5	1.75	0.02	b.d.l	-	45.48	0.28	14.43	0.08	9.52	0.05	11.9	0.26	0.07	0.02	15.04	0.12	0.76	0.01	0.14	0.01	n.m.	-	n.m.	-	99.38	0.55
Cu2-3	5	1.71	0.02	b.d.l	-	45.86	0.23	14.37	0.09	9.49	0.05	11.76	0.09	0.08	0.02	15.01	0.1	0.75	0.02	0.13	0.01	n.m.	-	n.m.	-	99.42	0.54
IS3-1	2	1.76	0.04	0.16	0.01	49.29	0.14	14.72	0.11	10.33	0.03	12.28	0.02	0.06	0.03	8.36	0.24	0.83	0.16	0.14	0.01	n.m.	-	n.m.	-	97.99	0.34
IS3-2	19	1.55	0.06	0.14	0.01	48.12	0.25	14.09	0.18	10.32	0.12	11.16	0.22	0.06	0.03	8.2	0.23	0.49	0.09	0.12	0.02	b.d.l.	-	0.72	0.11	95.11	2.83
IS4-1	20	1.76	0.05	1.64	0.03	50.6	0.31	16.07	0.17	9.15	0.08	10.53	0.07	0.04	0.03	7.1	0.17	0.66	0.07	b.d.l.	-	0.87	0.06	0.18	0.01	98.75	0.27
IS4-2	17	1.87	0.05	1.77	0.04	49.38	0.27	16.96	0.19	8.12	0.11	10.62	0.06	0.02	0.02	7.38	0.21	0.7	0.11	b.d.l.	-	1.07	0.05	0.17	0.03	98.25	0.27
IS4-3	15	2.06	0.07	2.21	0.07	50.51	0.2	18.23	0.14	6.49	0.28	8.99	0.14	0.02	0.02	7.28	0.19	0.79	0.11	b.d.l.	-	1.16	0.06	0.15	0.02	98.06	0.28
IS4-4	6	1.75	0.27	1.73	0.42	51.59	0.69	15.16	1.28	8.88	1.69	10.74	1.43	0.06	0.03	7.1	0.09	0.7	0.07	b.d.l.	-	0.84	0.05	0.28	0.17	99.22	0.75
IS4-6	28	1.67	0.05	1.57	0.02	50.71	0.2	15.65	0.11	9.47	0.13	10.99	0.08	0.03	0.03	6.68	0.11	0.58	0.09	b.d.l.	-	0.88	0.05	0.27	0.02	98.66	0.52
KK54	8	1.8	0.05	0.14	0.01	49.41	0.22	15.53	0.15	10.88	0.13	11.94	0.07	0.02	0.01	8.09	0.3	0.64	0.17	b.d.l.	-	0.52	0.05	0.61	0.05	99.71	0.89

* Total trace elements (oxides) derived from LA-ICPMS. EPMA data has been used in preference when above analytical detection limit.

b.d.l. – below detection limit.

n.m. – not measured.

Table S-4 Composition of the quenched silicate melt determined by LA-ICPMS.

Run #	n	MnO wt. %	σ	TiO$_2$ wt. %	σ	P ppm	σ	Cr ppm	σ	Ni ppm	σ	Cu ppm	σ	Zn ppm	σ	Ba ppm	σ
IS5-2	5	0.1	0.1	0.8	0.1	36	41	44	9	0.2	0.4	813	31	21373	262	58	3
IS7-1	8	0.2	0.2	0.8	0.1	16	22	427	28	110	22	427	28	15588	135	241	4
IS7-2	8	0.2	0.2	0.8	0.1	33	56	406	24	142	12	406	24	15553	424	476	10
Cu2-2	4	0.2	0.2	0.8	0.1	633	44	654	20	19.6	1.8	300	7	564	5	19	1
Cu2-3	4	0.2	0.2	0.8	0.1	570	50	611	10	21.5	1.1	362	6	538	17	17	1
IS3-1	1	0.1	0.1	0.8	0.1	612	-	288	-	3	-	14	-	367	-	57	-
IS3-2	6	0.1	0.1	0.8	0.1	553	135	263	13	0.9	0.6	16	2	344	14	22537	4095
IS4-1	7	0.2	0.2	0.8	0.1	93	108	88	10	206.8	16	28	3	6542	81	19	6
IS4-2	6	0.2	0.2	0.8	0.1	113	66	59	5	195.9	8.8	26	2	8245	187	39	3
IS4-3	2	0.2	0.2	0.9	0.1	121	24	37	3	291.7	185.1	23	4	8743	171	27	1
IS4-4	3	0.2	0.2	0.8	0.1	230	160	157	19	3490.8	317.5	184	9	7356	339	23	3
IS4-6	8	0.2	0.2	0.7	0.1	120	40	106	5	224.7	12.1	31	1	7040	120	2157	545
KK54	3	0.1	0.1	0.8	0.1	200	39	85	7	1.7	1.1	177	23	4176	154	6390	2850

The high-Ba content in IS3-2 glass originated from contamination by the BaCO$_3$ sleeve.

Table S-5 Zinc isotope compositions of experimental phases and USGS standards.

Run #	phase	$\delta^{66/64}$Zn (‰)	2SD	$\delta^{68/64}$Zn (‰)	2SD	n	Obtained by sample-standard bracketing				Obtained by sample-sample bracketing			
							$\Delta^{66/64}$Zn$_{metal/sulfide\text{-}silicate}$ (‰)	2SD	$\Delta^{68/64}$Zn$_{metal/sulfide\text{-}silicate}$ (‰)	2SD	$\Delta^{66/64}$Zn$_{metal/sulfide\text{-}silicate}$ (‰)	2SD	$\Delta^{68/64}$Zn$_{metal/sulfide\text{-}silicate}$ (‰)	2SD
IS5-2	silicate	-0.08	0.04	-0.13	0.03	3	0.05	0.05	0.08	0.09	0.03	0.03	0.04	0.08
	metal	-0.03	0.02	-0.05	0.09	3								
IS5-2 rep	silicate	-0.06	0.02	-0.1	0.01	3	0.03	0.02	0.06	0.02	-0.02	0.03	-0.04	0.02
	metal	-0.02	0.00	-0.03	0.01	3								
IS7-1	silicate	-0.005	0.020	-0.001	0.021	3	-0.011	0.032	-0.016	0.053	0.003	0.014	0.005	0.022
	metal	-0.016	0.026	-0.018	0.048	3								
IS7-2	silicate	-0.014	0.016	-0.022	0.021	3	-0.001	0.019	-0.005	0.024	-0.002	0.015	-0.004	0.013
	metal	-0.015	0.010	-0.027	0.012	3								
IS3-1	silicate	0.00	0.01	0.01	0.02	3	-0.15	0.02	-0.29	0.05	-0.17	0.05	-0.29	0.09
	sulfide	-0.15	0.02	-0.28	0.04	3								
IS3-2	silicate	-0.04	0.01	-0.08	0.01	3	-0.09	0.01	-0.16	0.03	-0.07	0.04	-0.13	0.06
	sulfide	-0.13	0.01	-0.25	0.02	3								
KK54	silicate	0.00	0.03	-0.05	0.04	3	-0.07	0.04	-0.05	0.06	-0.05	0.01	-0.11	0.01
	sulfide	-0.06	0.03	-0.11	0.04	3								
IS4-2	silicate	-0.02	0.01	0.01	0.07	3	-0.03	0.03	-0.06	0.09	-0.03	0.02	-0.09	0.09
	sulfide	-0.05	0.03	-0.05	0.06	3								
IS4-3	silicate	-0.02	0.02	-0.04	0.07	3	-0.04	0.05	-0.11	0.21	-0.06	0.03	-0.13	0.04
	sulfide	-0.06	0.05	-0.15	0.2	3								
IS4-4	silicate	-0.03	0.03	-0.06	0.11	3	-0.09	0.04	-0.19	0.11	-0.09	0.01	-0.18	0.08
	sulfide	-0.12	0.01	-0.25	0.03	3								
IS4-6	silicate	-0.03	0.03	-0.04	0.03	3	0.00	0.04	-0.03	0.03	-0.02	0.03	-0.04	0.02
	sulfide	-0.03	0.02	-0.07	0.02	3								
KK54 rep	silicate	-0.03	0.04	-0.03	0.07	3	-0.03	0.06	-0.06	0.11	-0.02	0.03	-0.04	0.02
	sulfide	-0.05	0.04	-0.09	0.08	3								

Table S-5 *Continued*

Run #	phase	$\delta^{66/64}$Zn (‰)	2SD	$\delta^{68/64}$Zn (‰)	2SD	n	Obtained by sample-standard bracketing				Obtained by sample-sample bracketing			
							$\Delta^{66/64}$Zn$_{\text{metal/sulfide-silicate}}$ (‰)	2SD	$\Delta^{66/64}$Zn$_{\text{metal/sulfide-silicate}}$ (‰)	2SD	$\Delta^{66/64}$Zn$_{\text{metal/sulfide-silicate}}$ (‰)	2SD	$\Delta^{68/64}$Zn$_{\text{metal/sulfide-silicate}}$ (‰)	2SD
USGS standards														
G-2		0.34	0.05	0.65	0.08	3								
BHVO-2		0.25	0.02	0.53	0.08	3								
AGV-1		0.28	0.02	0.55	0.02	3								
RGM-1		0.33	0.02	0.65	0.02	3								
BCR-2 @1		0.24	0.03	0.48	0.06	3								
BCR-2 @2		0.25	0.03	0.53	0.08	3								
NOD-P		0.8	0.03	1.59	0.04	2								
BIR-1 @1		0.28	0.04	0.57	0.08	2								
BIR-1 @2		0.3	0	0.59	0.02	2								
BIR-1 @3		0.27	0.05	0.55	0.02	2								

"rep" signifies replicate chemical purification and subsequent measurement of the same sample aliquot.

"@" represents independent dissolution, chemical purification, and measurement of powder splits.

Run products and USGS standards are reported as the relative deviation from NIST SRM 683 and JMC-Lyon, respectively.

Table S-6 Copper isotope compositions of experimental phases and USGS standards.

Run #	phase	$\delta^{65/63}$Cu (‰)	2SD	n	Obtained by standard bracketing		Obtained by sample bracketing	
					$\Delta^{65/63}Cu_{metal/sulfide-silicate}$ (‰)	2SD	$\Delta^{65/63}Cu_{metal/sulfide-silicate}$ (‰)	2SD
IS5-2	silicate	0.26	0.02	3	0.25	0.03		
	metal	0.51	0.03	3				
IS7-1	silicate	0.25	0.02	3	0.18	0.03		
	metal	0.43	0.02	3				
IS7-2	silicate	0.16	0.04	3	0.07	0.05		
	metal	0.23	0.02	3				
Cu2-2	silicate	0.37	0.02	3	-0.33	0.05		
	sulfide	0.04	0.05	3				
Cu2-3	silicate	0.38	0.02	3	-0.25	0.03		
	sulfide	0.14	0.02	3				
IS3-1	silicate	0.65	0.03	3	-0.23	0.04		
	sulfide	0.42	0.03	3				
IS3-2	silicate	0.56	0.01	3	-0.15	0.02		
	sulfide	0.41	0.02	3				
KK54	silicate	0.65	0.03	3	-0.06	0.05		
	sulfide	0.59	0.04	3				
IS4-1	silicate	0.75	0.03	3	-0.04	0.04	-0.01	0.02
	sulfide	0.71	0.03	3				
IS4-2	silicate	0.70	0.04	3	-0.03	0.06	0.01	0.04
	sulfide	0.67	0.05	3				
IS4-3	silicate	0.72	0.04	3	-0.02	0.06	0.01	0.02
	sulfide	0.70	0.05	3				
IS4-4	silicate	0.79	0.04	3	-0.15	0.06	-0.15	0.02
	sulfide	0.64	0.04	3				

Table S-6 *Continued*

Run #	phase	$\delta^{65/63}$Cu (‰)	2SD	n	Obtained by standard bracketing		Obtained by sample bracketing	
					$\Delta^{65/63}Cu_{metal/sulfide-silicate}$ (‰)	2SD	$\Delta^{65/63}Cu_{metal/sulfide-silicate}$ (‰)	2SD
USGS standards								
BCR-2		0.20	0.02	3				
AGV-1 @1		0.04	0.04	3				
AGV-1 @2		0.02	0.04	3				
AGV-1 @3		0.03	0.05	3				
BHVO-2 @1		0.14	0.02	3				
BHVO-2 @2		0.16	0.05	3				
NOD-P @1		0.40	0.03	3				
NOD-P @2		0.41	0.04	3				
NOD-P @3		0.37	0.05	3				
NOD-A		0.30	0.04	3				
BIR-1 @1		0.10	0.04	3				
BIR-1 @2		0.11	0.01	3				

"@" represents independent dissolution, chemical purification, and measurement of powder splits.

Supplementary Figures

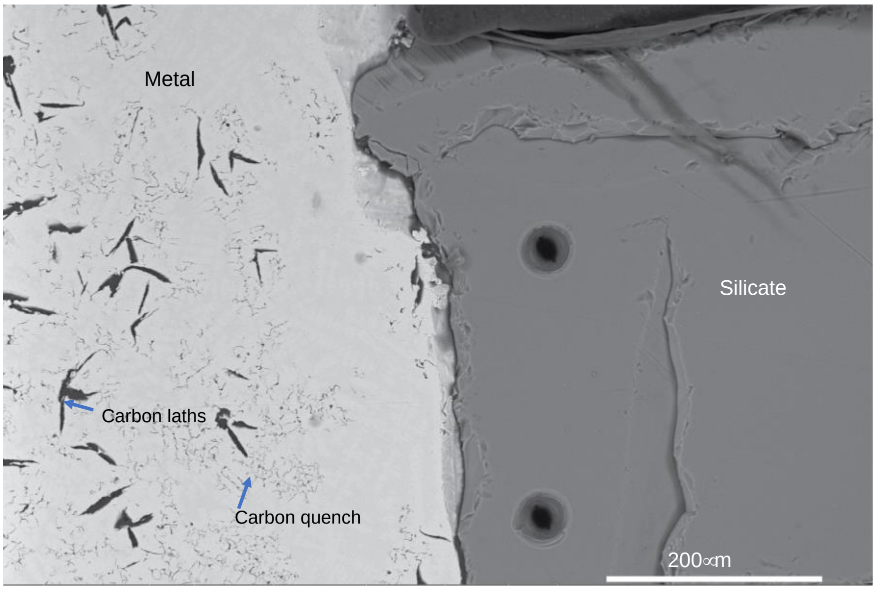

Figure S-1 Backscattered electron (BSE) image of the iron-rich experiment 7-1, showing the carbon-rich metallic phase (left), with both precipitated carbon laths and exsolved carbon quench, and the silicate phase (right). Holes in the silicate portion are laser ablation pits.

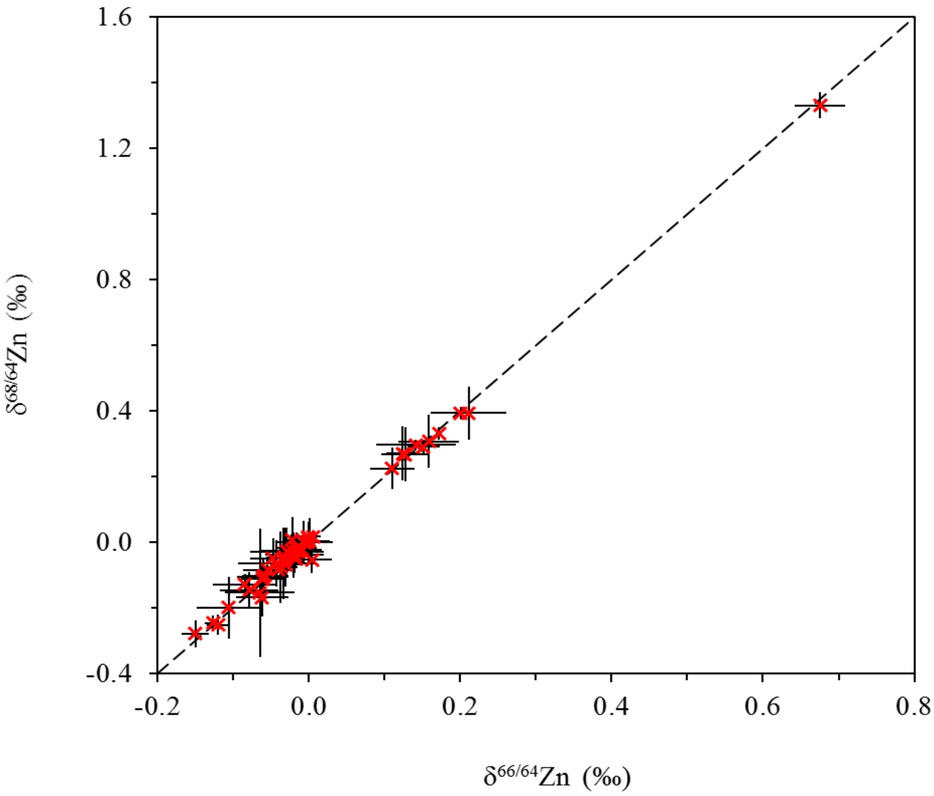

Figure S-2 Plot showing the linear correlation between $\delta^{68/64}$Zn and $\delta^{66/64}$Zn in USGS standards and run products including sulphide, silicate, and metal phases. Data are reported in Table S-5.

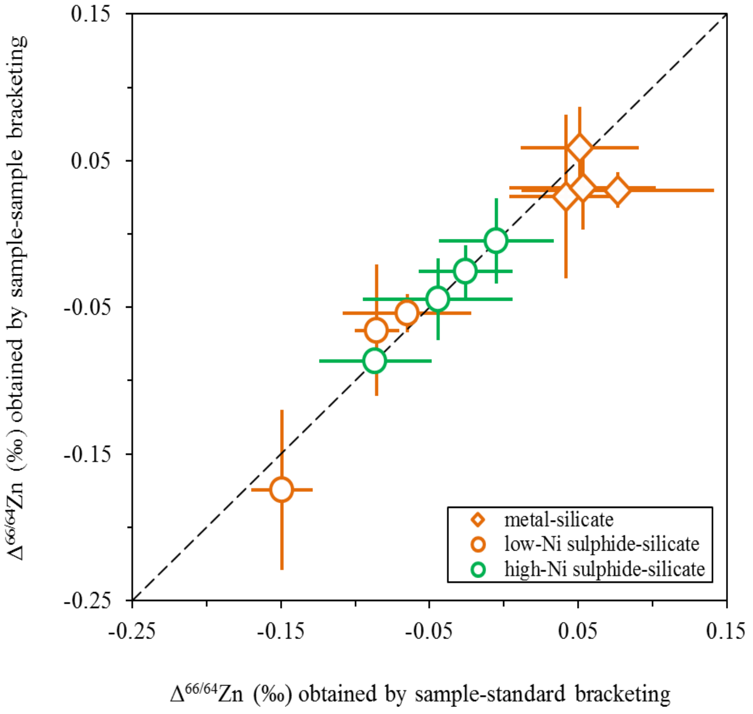

Figure S-3 Comparison of the Zn isotope fractionation factors obtained by conventional sample-standard bracketing and a novel method named as "sample-sample bracketing" (see methods for detail). Data obtained by both methods are identical within errors.

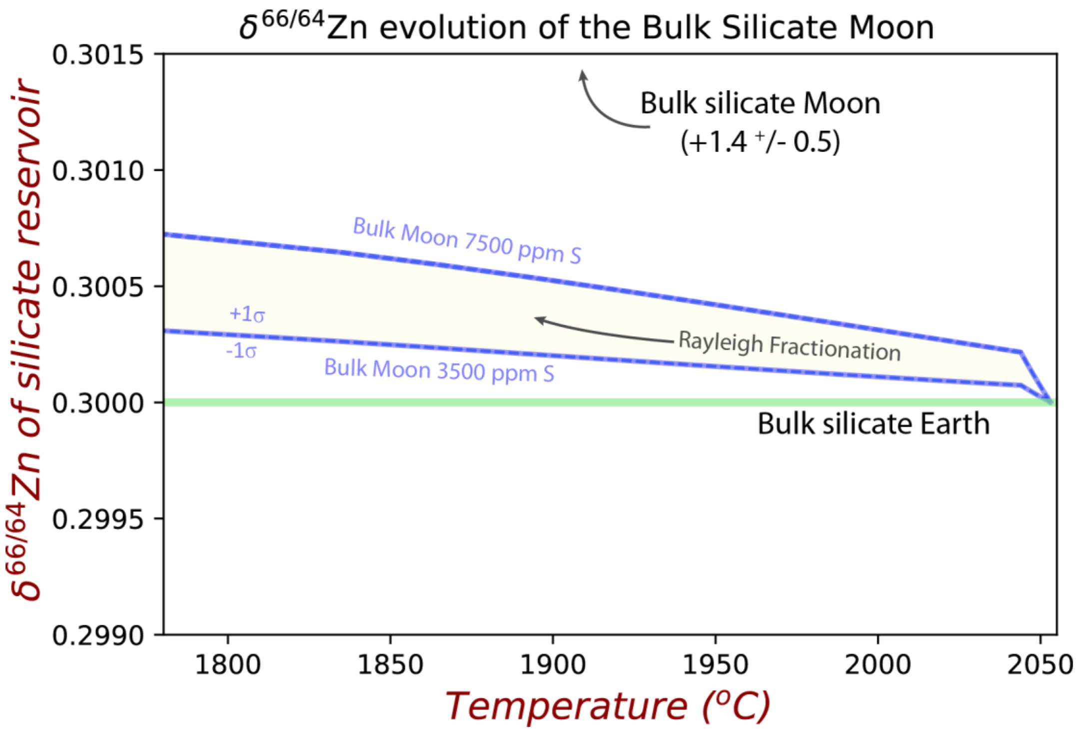

Figure S-4 The silicate Moon's Zn isotope composition is essentially unaffected by lunar sulfide segregation to its core. This assumes the Moon is derived from the precursor BSE, and the Moon's core is predominantly FeS (equating to a bulk Moon of ~7500 ppm S), or just the outer core (3500 ppm S) and sulfide sequestration occurs by Rayleigh fractionation. The green horizontal line represents the values of the BSE (Paniello *et al.*, 2012), with lunar values taken from Kato *et al.* (2015). The pale blue band represents 1 standard deviations of the error on the mean of the fractionation regression.

Supplementary Information References

Bridgestock, L., Williams, H., Rehkämper, M., Larner, F., Giscard, M., Hammond, S., Coles, B., Andreasen, R., Wood, B., Theis, K. (2014) Unlocking the zinc isotope systematics of iron meteorites. *Earth and Planetary Science Letters* 400, 153-164.

Chen, S., Liu, Y., Hu, J., Zhang, Z., Hou, Z., Huang, F., Yu, H. (2016) Zinc isotopic compositions of NIST SRM 683 and whole-rock reference Materials. *Geostandards and Geoanalytical Research*.

Craddock, P.R., Warren, J.M., Dauphas, N. (2013) Abyssal peridotites reveal the near-chondritic Fe isotopic composition of the Earth. *Earth and Planetary Science Letters* 365, 63-76.

Danyushevsky, L.V., Plechov, P. (2011) Petrolog3: Integrated software for modeling crystallization processes. *Geochemistry Geophysics Geosystems* 12.

Elardo, S.M., Shahar, A. (2017) Non-chondritic iron isotope ratios in planetary mantles as a result of core formation. *Nature Geoscience* 10, 317-321.

He, Z., Huang, F., Yu, H., Xiao, Y., Wang, F., Li, Q., Xia, Y., Zhang, X. (2016) A flux-free fusion technique for rapid determination of major and trace elements in silicate rocks by LA-ICP-MS. *Geostandards and Geoanalytical Research* 40, 5-21.

Herzog, G., Moynier, F., Albarède, F., Berezhnoy, A. (2009) Isotopic and elemental abundances of copper and zinc in lunar samples, Zagami, Pele’s hairs, and a terrestrial basalt. *Geochimica Et Cosmochimica Acta* 73, 5884-5904.

Huang, J., Huang, F., Wang, Z., Zhang, X., Yu, H. (2017) Copper isotope fractionation during partial melting and melt percolation in the upper mantle: Evidence from massif peridotites in Ivrea-Verbano Zone, Italian Alps. *Geochimica Et Cosmochimica Acta* 211, 48-63.

Kato, C., Moynier, F. (2017) Gallium isotopic evidence for extensive volatile loss from the Moon during its formation. *Science Advances* 3, e1700571.

Kato, C., Moynier, F., Valdes, M.C., Dhaliwal, J.K., Day, J.M.D. (2015) Extensive volatile loss during formation and differentiation of the Moon. *Nature Communications* 6, 7617.

Kiseeva, E.S., Wood, B.J. (2013) A simple model for chalcophile element partitioning between sulphide and silicate liquids with geochemical applications. *Earth and Planetary Science Letters* 383, 68-81.

Kiseeva, E.S., Wood, B.J. (2015) The effects of composition and temperature on chalcophile and lithophile element partitioning into magmatic sulphides. *Earth and Planetary Science Letters* 424, 280-294.

Liu, Y., Hu, Z., Gao, S., Günther, D., Xu, J., Gao, C., Chen, H. (2008) In situ analysis of major and trace elements of anhydrous minerals by LA-ICP-MS without applying an internal standard. *Chemical Geology* 257, 34-43.

Mahan, B., Siebert, J., Pringle, E.A., Moynier, F. (2017) Elemental partitioning and isotopic fractionation of Zn between metal and silicate and geochemical estimation of the S content of the Earth’s core. *Geochimica Et Cosmochimica Acta* 196, 252-270.

McDade, P., Wood, B.J., Westrenen, W.V., Brooker, R., Gudmundsson, G., Soulard, H., Najorka, J., Blundy, J. (2002) Pressure corrections for a selection of piston-cylinder cell assemblies. *Mineralogical Magazine* 66, 1021-1028.

McDonough, W.F., Sun, S.-s. (1995) The composition of the Earth. *Chemical Geology* 120, 223-253.

Moynier, F., Vance, D., Fujii, T., Savage, P. (2017) The isotope geochemistry of zinc and copper. *Reviews in Mineralogy and Geochemistry* 82, 543-600.

Paniello, R.C., Day, J.M., Moynier, F. (2012) Zinc isotopic evidence for the origin of the Moon. *Nature* 490, 376-9.

Pringle, E.A., Moynier, F. (2017) Rubidium isotopic composition of the Earth, meteorites, and the Moon: Evidence for the origin of volatile loss during planetary accretion. *Earth and Planetary Science Letters* 473, 62-70.

Righter, K., Drake, M.J. (1996) Core Formation in Earth's Moon, Mars, and Vesta. *Icarus* 124, 513-529.

Savage, P.S., Moynier, F., Chen, H., Shofner, G., Siebert, J., Badro, J., Puchtel, I. (2015) Copper isotope evidence for large-scale sulphide fractionation during Earth’s differentiation. *Geochemical Perspectives Letters*.

Smythe, D.J., Wood, B.J., Kiseeva, E.S. (2017) The S content of silicate melts at sulfide saturation: new experiments and a model incorporating the effects of sulfide composition. *American Mineralogist* 102, 795-803.

Wade, J., Wood, B.J. (2016) The oxidation state and mass of the Moon-forming impactor. *Earth and Planetary Science Letters* 442, 186-193.

Wang, K., Jacobsen, S.B. (2016) Potassium isotopic evidence for a high-energy giant impact origin of the Moon. *Nature* 538, 487-490.

Weber, R.C., Lin, P.Y., Garnero, E.J., Williams, Q., Lognonne, P. (2011) Seismic detection of the lunar core. *Science* 331, 309-12.

Wood, B.J. (1993) Carbon in the core. *Earth and Planetary Science Letters* 117, 593-607.